Biotechnology and Applied Biochemistry

A new generation of sodium chloride porogen for tissue engineering

Richard T. Tran,[1] Elhum Naseri,[1] Aleksey Kolasnikov,[1] Xiaochun Bai,[2,3] and Jian Yang[1]*

[1]*Department of Bioengineering, The University of Texas at Arlington, Arlington, TX, USA*

[2]*Department of Cell Biology, School of Basic Medical Science, Southern Medical University, Guangzhou, People' s Republic of China*

[3]*Research Institute of Orthopedic, Southern Medical University, Guangzhou, People' s Republic of China*

Abstract.

Porogen leaching is a widely used and simple technique for the creation of porous scaffolds in tissue engineering. Sodium chloride (NaCl) is the most commonly used porogen, but the current grinding and sieving methods generate salt particles with huge size variations and cannot generate porogens in the submicron size range. We have developed a facile method based on the principles of crystallization to precisely control salt crystal sizes down to a few microns within a narrow size distribution. The resulting NaCl crystal size could be controlled through the solution concentration, crystallization temperature, and crystallization time. A reduction in solution temperature, longer crystallization times, and an increase in salt concentration resulted in an increase in NaCl crystal sizes due to the lowered solubility of the salt solution. The nucleation and crystallization technique provides superior control over the resulting NaCl size distribution (13.78 $\pm$ 1.18 μm), whereas the traditional grinding and sieving methods produced NaCl porogens 13.89 $\pm$ 12.49 μm in size. The resulting NaCl porogens were used to fabricate scaffolds with increased interconnectivity, porous microchanneled scaffolds, and multiphasic vascular grafts. This new generation of salt porogen provides great freedom in designing versatile scaffolds for various tissue-engineering applications.

Volume 58, Number 5, September/October 2011, Pages 335–344 •
E-mail: jianyang@uta.edu; baixc15@smu.edu.cn

Keywords: elastomer, porogen, microelectromechanical systems, scaffold, vascular graft

1. Introduction

Tissue engineering is a multidisciplinary field that aims to provide therapeutic treatments to maintain, restore, or replace damaged or diseased tissues, and may one day provide better alternatives for whole organ transplantation [1],[2]. Within the past decade, monumental strides have been made in the regeneration of various tissues such as skin [3], bone [4], cartilage [5], tendons [6], ligaments [7], liver [8], cardiac tissues [9], blood vessels [10], esophagus [11], adipose [12], renal [13], lung [14], and neural tissues [15]. One of the principal methods behind tissue engineering involves growing relevant cells into a three-dimensional (3D) tissue or organ. However, cells alone lack the ability to grow into 3D orientations that are similar to the native tissues. Therefore, the preferred multidimensional cellular growth is achieved by seeding the desired cells onto porous matrices, known as scaffolds, which serve as a temporary extracellular matrix (ECM) during new tissue formation [16]. This temporary ECM is not only responsible for defining the 3D architecture of the construct, but also plays a large role in regulating cellular phenotype and functional properties through the dynamic interplay between the cells and ECM structure [17]. Thus, by mimicking the native ECM and serving as a temporary suitable microenvironment for initial cell attachment and 3D tissue formation, the scaffold has become a very important component of the tissue engineering paradigm with its ability to influence cellular behavior and ultimately determine the success of the tissue-engineered construct [18].

The requirements for tissue engineering scaffolds are multifaceted and tissue specific. In general, tissue engineering scaffolds should be biocompatible in that cell attachment, differentiation, and proliferation should all be promoted while minimizing the host foreign body response to the implanted construct [19]. Scaffolds should also degrade to match the rate of new tissue

Abbreviations: 2D, two dimensional; 3D, three dimensional; CAD, computer-aided design; CUPE, crosslinked urethane doped polyester; ECM, extracellular matrix; FTIR, Fourier transform infrared spectroscopy; HDI, 1,6-hexamethyl diisocyanate; MEMS, microelectromechanical systems; NaCl, sodium chloride; PDMS, polydimethylsiloxane; POC, poly(octanediol citrate); SEM, scanning electron microscope; TIPS, thermally induced phase separation.

*Address for correspondence: Dr. Jian Yang, PhD, Associate Professor of Bioengineering, Department of Bioengineering, The University of Texas at Arlington, 500 UTA Boulevard, Arlington, TX 76010, USA. Tel: +817-272-0562; Fax: +817-272-2251; e-mail: jianyang@uta.edu. Dr. Xiaochun Bai, Department of Cell Biology, School of Basic Medical Science, Southern Medical University, Guangzhou 510515, China. E-mail: baixc15@smu.edu.cn.

Received 17 May 2011; accepted 13 July 2011
DOI: 10.1002/bab.44
Published online 16 September 2011 in Wiley Online Library (wileyonlinelibrary.com)

formation, and precisely match the mechanical properties of the surrounding tissues to avoid compliance mismatch, which has been shown to be a major cause of implant failure [20]. In addition to biological and biomechanical performance, the scaffold must also possess key morphological characteristics. Scaffold morphologies should resemble the micro/nanoscale architectures of the native ECM [21], and consist of a highly interconnected porous network, which can encourage cellular infiltration and allow for the proper exchange of nutrients and metabolic waste throughout the scaffold [22],[23]. As the resulting scaffold morphology characteristics are primarily determined by the fabrication method used to create them, intense research focus has now shifted toward developing new fabrication methodologies to control the scaffold pore size [24], shape [25], porosity [26], and interconnectivity [27] for various tissue engineering applications.

For example, thermally induced phase separation (TIPS) methods have been extensively studied and rely on the principle that a solvent's effectiveness will decrease when introduced into a nonsolvent or when the temperature of the system is lowered [28],[29]. Although the creation of pore sizes in the range of nanometers [30] to a few micrometers [31] can be obtained, the phase separation technique cannot produce pore sizes in the upper micrometer size range, which limits its use in applications involving skin or bone where the required pore sizes are 20–400 μm [32]. Thus, phase separation techniques must be combined with other methods such as porogen leaching to be realized in a wider variety of applications [33]. Another frequently used method in the fabrication of porous scaffolds for tissue engineering is a foaming process technique [34], which utilizes foaming agents such as water [35], carbon dioxide [36], nitrogen [37], or fluoroforms [38] as expanding substances to generate pores. Although the foaming method is relatively inexpensive and a wide range of pore sizes (30–700 μm) [39] can be obtained, this process is generally plagued by the creation of "dead" or closed-pore structures leading to very low levels of interconnectivity [40]. The foaming technique, similar to phase separation methods, must be combined with porogen leaching techniques to increase porosity and interconnectivity [41].

Other methods developed to precisely control the resulting scaffold pore size and shape rely on a computer-aided design (CAD) data set [42]. For example, rapid prototyping [43], solid freeform fabrication [16], 3D printing [44], shape deposition manufacturing [45], fused deposition modeling [46], selective laser sintering [47], and stereolithographic principles all use a step-by-step, layer-by-layer construction mechanism to fabricate scaffolds with highly reproducible and precisely controlled porosities, interconnectivity, pore sizes, and pore shapes. However, these methods are restricted in terms of the resolution of the engineered machine tools used (200–500 μm) [48], lengthy fabrication times [49], costly/complex fabrication methods, small final scaffold sizes (0.4–3.5 cm^3) [50], and the demand for specific scaffold material properties [51]. Another established process for the fabrication of tissue engineering scaffolds is an electrospinning process, which produces fibers in the micrometer or nanometer scale by electrically charging a suspended droplet of polymer solution. Nonwoven two-dimensional (2D) fiber meshes can be constructed into 3D fibrous meshes with a wide range of pore size distributions and porosities with a high surface area-to-volume ratio [52]. However, similar to phase separation methods and techniques utilizing CAD designs, the electrospinning process places a demand for specific scaffold material properties, which limits the scope of these fabrication methods to select biomaterials [51]. For example, low-molecular-weight biodegradable elastomers such as poly(octanediol citrate) (POC) [53], poly(octamethylene maleate anhydride citrate) [54–56], and poly(glycerol sebacate) [57] cannot be used in these methods to fabricate porous scaffolds.

Unlike the previous methods mentioned above, porogen leaching, also known as solution casting/particulate leaching, is a widely used, facile, convenient, and cost-effective method that can be applied with a wide range of polymers to introduce porosity into tissue engineering scaffolds [58]. This method involves the casting of a polymer/porogen solution followed by solvent evaporation and removal of the incorporated porogen through aqueous washing methods. Various porogens, including sodium chloride (NaCl) [59], paraffin spheres [60], sugar crystals [61], gelatin [62], and polymers [63], have been successfully used to fabricate porous structures. NaCl is perhaps the most widely used porogen, but the wide variations of pore sizes, lack of interconnectivity, irregular pore geometry, and the inability to produce submicron and nanoscale pore sizes have limited the use of this porogen in current tissue engineering applications. Therefore, a convenient, cost-effective pore creation technology to fabricate scaffolds with controlled architectures and that can be applied to a wide range of biomaterials would be a valuable tool for the field of tissue engineering.

Crystallization is a process that occurs naturally in the formation of minerals and snowflakes, and has been utilized in industrial settings for the past 30 years to produce salts, powders, and silicon crystal wafers [64]. Recent research involving nucleation and crystallization science has been directed toward a variety of biological applications, including protein research [65] and the fabrication of microstructures and nanoparticles [66]. The process of crystallization (Fig. 1A) is based upon a change in phase of a material from a solvated state to a crystal lattice structure due to a reduction in free energy of the solution. As the transition from high to low free energy occurs, the solute molecules cluster into nuclei in the nanometer scale in a process termed "nucleation" (Fig. 1A-3). Once the nuclei reach a critical size, the molecules of the solute rearrange into a crystal structure, and crystal growth is initiated (Fig. 1A-4) [67]. We hypothesize that controlling specific parameters of the crystallization process such as the nature of the solute, supersaturation level, solution temperature, stirring/mixing, and crystal growth time can potentially produce crystals with a high level of control over the shapes and sizes for tissue engineering scaffold fabrication [64],[67].

The rationale behind this approach is that 1) crystallization technology can be used to generate NaCl porogens of a controlled size with a narrow size distribution to fabricate tissue engineering scaffolds with better control over porosity and pore size; 2) crystallization technology can be used to generate pores of a distinct shape to create scaffolds with regular pore geometry; 3) crystallization can allow for the

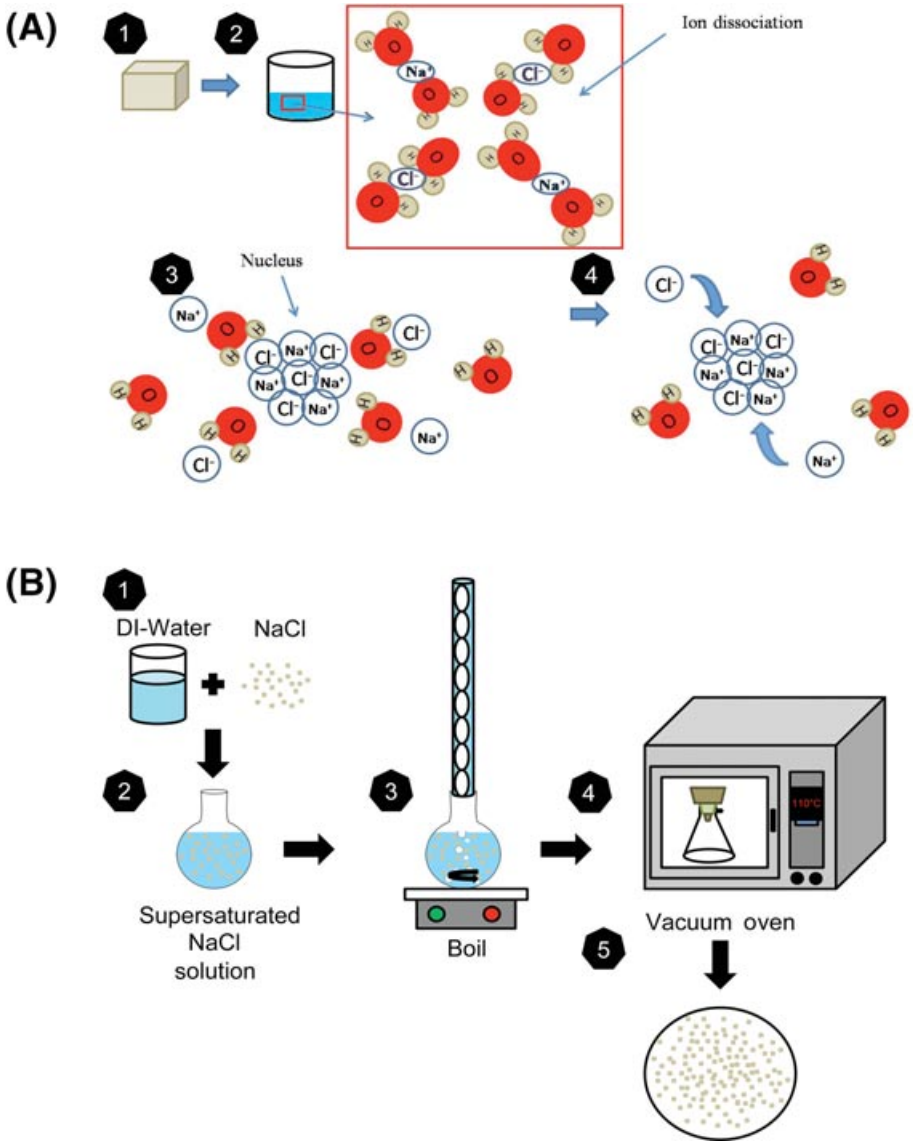

Fig. 1. (A) Schematic representation of the nucleation and crystallization process. (1) NaCl salt is combined with water and (2) dissolved by ion dissociation. (3) Under a reduction of solution free energy, the dissociated ions are driven to form a nucleus. (4) Upon further reduction of free energy of the solution results in crystal growth. (B) Schematic representation of NaCl nucleation and crystallization experimental setup. (1) NaCl salt and deionized water is combined into a round bottom flask to create a supersaturated solution. (2) The temperature of the supersaturated solution is elevated until the salt is completely dissolved. (3) The temperature of the system is then reduced to initiate nuclei formation and crystal growth. (4) The crystallized salt is then vacuum filtered in an oven maintained at the respective nucleation temperature, and collected from the filter paper (5).

generation of NaCl porogens in the submicron and nanoscale range to fabricate scaffolds with topographies that better mimic the native ECM; 4) incorporation of the submicron NaCl with other fabrication methods will increase the interconnectivity of the resulting scaffold for enhanced cellular communication and mass transport; 5) the salt generated in this technique can be applied with microelectromechanical system (MEMS)-based technologies to control cellular organization while providing a means for cell communication; 6) unlike some of the previous techniques, this scaffold fabrication process used in this technique can be applied to a wide variety of materials; and 7) this pore technology is easy, convenient, cost-effective, and does not require the use of complex machinery, which facilitates widespread use in academic laboratories and industry.

The aim of the present study is to explore the feasibility of using the principles behind crystallization to create NaCl porogens, which can be used to address the limitations of previous ground and sieved porogens for various biomedical applications. We focus on characterizing the effects of various crystallization parameters such as solution concentration, solution temperature, and crystallization time on the resulting NaCl crystal size. To show the feasibility and future potential of this

new pore generation technique, the resulting NaCl porogens produced were used to increase the interconnectivity of traditional salt-leached scaffolds, and the fabrication of microchanneled elastomeric scaffolds and multiphasic vascular grafts.

2. Materials and methods

2.1. Materials

All materials were purchased from Fisher Scientific (Pittsburgh, PA, USA), and all chemicals were purchased from Sigma–Aldrich (St. Louis, MO, USA) unless specified otherwise and used as received.

2.2. NaCl porogen fabrication

NaCl porogens were fabricated according to the schematic representation shown in Fig. 1B. Briefly, NaCl salt (99.0% purity) was dissolved in deionized water produced from a Direct-Q Water Purification System (Millipore, Billerica, MA, USA) at various concentrations above the supersaturation level at 25°C. The supersaturated NaCl solution was placed in a round bottom glass flask fitted with a magnetic pear-shaped stir bar. The flask containing the supersaturated solution was then lowered into an oil bath maintained at 115°C. The contents were stirred at 400 rpm, and allowed to boil under reflux. After 30 Min, the temperature of the system was reduced to predetermined crystallization temperatures and allowed to stir for predetermined crystallization times to initiate nuclei formation and crystal growth. Following the end of the crystallization time period, the contents of the flask were filtered in an oven maintained at the respective crystallization temperature to collect the salt crystals. Various NaCl solution concentrations, crystallization times, and crystallization temperatures were studied to determine the effects on the resulting NaCl crystal size and shape.

2.3. Porogen characterization

The collected NaCl porogens were dried under vacuum, sputter coated with silver, and examined under a Hitachi S-3000N scanning electron microscope (SEM) (Hitachi, Pleasanton, CA, USA). Image J analysis software was used to determine the salt porogen sizes. To characterize the salt porogen geometries, 10 random locations were selected and a total of 30 measurements (latitudinal and longitudinal widths) were recorded at each location.

2.4. Crosslinked urethane-doped polyester synthesis

Crosslinked urethane-doped polyester (CUPE) pre-polymers were synthesized in two distinct steps similar to previously published methods [68]. The first step involves the synthesis of a pre-POC oligomer, which is chain extended by 1,6-hexamethyl diisocyanate (HDI) in the second urethane-doping step. Briefly, a POC pre-polymer was first synthesized by reacting a 1.0:1.1 monomer ratio of citric acid and 1,8-octanediol, respectively, in a three-necked round bottom flask fitted with an inlet and outlet adapter at 160°C under a constant flow of nitrogen [53]. Once all the monomers had melted, the temperature of the system was lowered to 140°C, and the reaction mixture was allowed to continue for 60 Min to create the POC pre-polymer. The POC pre-polymer was then purified by dropwise precipitation in deionized water. The undissolved pre-polymer was collected and lyophilized for 48 H to obtain the pre-POC oligomer (molecular weight 820 Dalton). In the second step, pre-CUPE was synthesized through the chain extension of the pre-POC. Pre-POC was dissolved in 1,4-dioxane (3.0 wt%), and the resulting solution was allowed to react with HDI in a clean reaction flask under constant stirring at 55°C using stannous octoate as a catalyst (0.1 wt%).

2.5. Traditional scaffold fabrication

To fabricate traditional NaCl salt-leached scaffolds, pre-CUPE was mixed with NaCl salt with an average crystal size in the range of 150–250 μm in a 1:10 polymer-to-salt ratio by weight using traditional grinding and sieving methods. The pre-polymer solution was mixed until a viscous paste was formed. The resulting slurry was placed in a Teflon mold, placed in a laminar flow hood overnight for solvent evaporation, and then transferred to an oven maintained at 80°C to crosslink the polymer through the condensation of pendant citric acid —COOH and —OH on the polymer backbone or branches. Next, the salt was leached out by immersion in deionized water for 72 H with water changes every 12 H. Finally, the resulting scaffolds were lyophilized for 36 H to remove any traces of water.

2.6. Interconnected scaffold fabrication

To fabricate traditional scaffolds with improved interconnectivity, pre-CUPE was mixed with equal amounts of NaCl salt (average crystal size in the range of 150–250 μm from traditional grinding and sieving methods) in combination with NaCl salt (average crystal size in the range of 1–10 μm from nucleation and crystallization) in a 1:10 polymer-to-combined salt ratio by weight. The pre-polymer solution was mixed until a viscous paste was formed. The resulting slurry was placed in a Teflon mold, placed in a laminar flow hood overnight for solvent evaporation, and then transferred to an oven maintained at 80°C to crosslink the polymer. Next, the salt was leached out by immersion in deionized water for 72 H with water changes every 12 H. Finally, the resulting scaffolds were lyophilized for 36 H to remove any traces of water.

2.7. Porous microchanneled scaffold fabrication

Microchanneled scaffolds were fabricated similarly to previously published methods [54]. The microchannel pattern was transferred from polydimethylsiloxane (PDMS) molds to CUPE. Briefly, pre-CUPE was mixed with NaCl salt with an average crystal size in the range of 1–10 μm in a 1:5 polymer-to-salt ratio by weight using nucleation and crystallization methods. The pre-polymer solution and salt were cast onto the PDMS microchannel mold and placed under vacuum to remove any air trapped in the channels. The microchannels filled with polymer and salt were then transferred to an oven maintained at 80°C to crosslink the polymer. Next, the salt was leached out by

immersion in deionized water for 72 H with water changes every 12 H. Finally, the microchanneled scaffolds were lyophilized for 36 H to remove any traces of water.

2.8. Multiphasic small diameter graft fabrication

Briefly, 3 mm outside diameter steel rods (McMaster-Carr, Atlanta, GA, USA) were dipped once into a dilute solution of pre-CUPE in 1,4-dioxane (1.0 wt%). Before the solution could dry, the rods were coated with the salt porogen created from nucleation and crystallization methods with an average pore size in the range of 1–10 μm. After the salt application, the rods were coated one additional time with pre-CUPE. Following the fabrication of the elastic membrane, a pre-CUPE solution was mixed with NaCl salt with an average crystal size in the range of 150–250 μm in a 1:10 polymer-to-salt ratio by weight using traditional grinding and sieving methods. The polymer solution was mixed thoroughly with the salt until a viscous paste was formed. The resulting slurry was cast onto the steel rods, and then placed in a laminar flow hood overnight for solvent evaporation. Once the solvent was removed, the scaffolds were post-polymerized in an oven maintained at 80°C to crosslink the polymer. Next, the salt in the tubular scaffold was leached out by immersion in deionized water for 72 H with water changes every 12 H. The scaffolds were removed from the steel rods by immersion in 50% ethanol. Finally, the scaffolds were lyophilized for 36 H to remove any residual water.

2.9. Scaffold geometry characterization

To view the cross-sectional morphology, scaffold samples were freeze fractured using liquid nitrogen, sputter coated with silver, and examined under SEM. Image J analysis software was used to determine the scaffold geometries. To characterize the scaffold geometries, three random locations were selected and a total of 30 measurements were recorded at each location.

The individual sections of the scaffold porosity were measured using the Archimedes' Principle, similar to previously published methods [69]. Briefly, a density bottle was used to measure the density and porosity of the scaffold using ethanol (density ρ_e) as the displacement liquid at 30°C. The density bottle filled with ethanol was weighed (W_1). A scaffold sample of weight W_S was immersed into the density bottle, and the air trapped in the scaffold was evacuated under vacuum. Next, the density bottle was supplemented with ethanol, filled, and weighed (W_2). The ethanol-saturated scaffold was removed from the density bottle, and the density bottle was weighed (W_3). The following parameters of the scaffold were calculated: the volume of the scaffold pore (V_P), the volume of the scaffold skeleton (V_S), the density (ρ_S), and the porosity (ε). The following formulas for the volume mass index (V_P/V_S) were used [69]:

$$V_P = (W_2 - W_3 - W_S)/\rho_e$$

$$V_S = (W_1 - W_2 - W_S)/\rho_e$$

$$\rho_S = W_S/V_S = W_S\rho_e/(W_1 - W_2 + W_S)$$

$$\varepsilon = V_P/(V_P + V_S) = (W_2 - W_3 - W_S)/(W_1 - W_3)$$

Scaffold interconnectivity was determined with Image J software. Briefly, the total area of a pore (A_t) and the area of each micropore above 20 μm in diameter (A_1, A_2, A_3, etc.) were calculated. The interconnectivity index was defined as described by previous methods [70]:

$$\text{Interconnectivity Index (\%)} = \frac{\text{Total Area of Micropores } (A_1 + A_2 + A_3 + \cdots)}{\text{Total Area } (A_t)} \times 100$$

The interconnectivity index for all the different pores in the image was calculated and an average of this value was taken as the final value. More than 10 SEM pictures for each sample were analyzed.

2.10. Statistical methods

Data were expressed as the mean $\pm$ standard deviation. The statistical significance between two sets of data was calculated using a two-tail Student's *t*-test. Nonparametric one-way analysis of variance tests were also performed where appropriate. Data were taken to be significant when a $P < 0.05$ was obtained.

3. Results and discussion

A new generation of NaCl porogen was created to address the limitations of previous porogen leaching designs. The principles behind nucleation and crystallization science were used as a means to produce NaCl crystals with control over the resulting porogen shape and size within a narrow size distribution, which is not possible using the current grinding and sieving methods. By controlling the free energy of the NaCl solution through the supersaturation concentration and nucleation temperature, various NaCl shapes and size distributions were created, which can be used in a wide variety of tissue engineering scaffold applications, where the pore size, porosity, and interconnectivity need to be precisely controlled to meet the tissue-specific requirements for proper regeneration.

Scanning electron microscope images for NaCl porogens nucleated at various concentrations at a fixed crystallization temperature (95°C) are shown in Figs. 2A–2C. The results show that the resulting NaCl porogen shape could be controlled through the solubility of the NaCl. At a lower concentration (0.36 g/mL), the NaCl porogens were spherical in morphology (Fig. 2A). As the concentration of the NaCl increased (0.37 and 0.38 g/mL), the resulting NaCl crystals were rhomboidal and cuboidal in geometry, respectively. The resulting NaCl porogen geometry was ultimately dictated by the solubility, or concentration of the supersaturated solution, which ultimately affected the crystal growth. As the NaCl nuclei are initiated through the reduction of free energy (temperature reduction), the porogen shapes become spherical in shape. Using the same conditions, a further reduction in free energy through the increased supersaturated concentrations initiated the crystal growth phase, resulting in the rhomboidal and final cuboidal geometries.

The resulting NaCl porogen size could also be controlled through the nucleation temperature. Figures 2D–2I show the

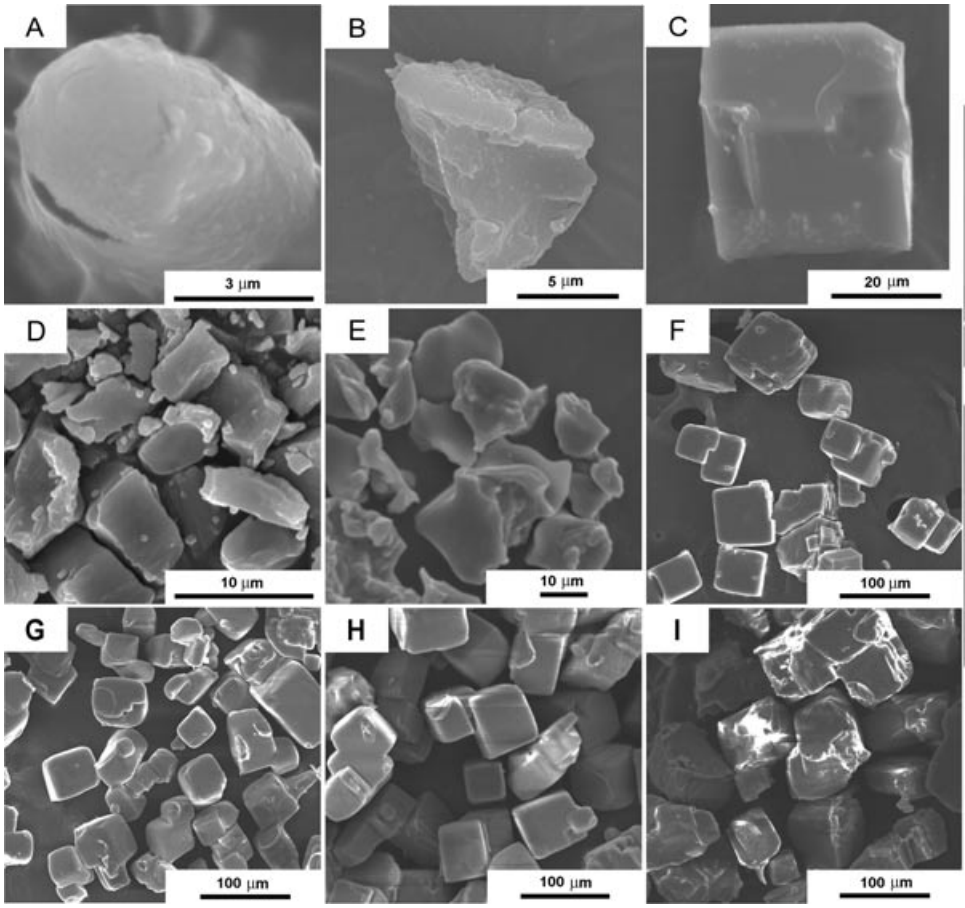

Fig. 2. SEM images of NaCl salt crystallized at different conditions to show control over porogen shape. (A) At higher solubility (0.36 g/mL), NaCl crystals take on spherical crystal morphology. As the solubility decreases (0.37 g/mL), NaCl crystals then take on a rhomboidal morphology (B), and result in a final cuboidal morphology (0.38 g/mL) (C). SEM images of NaCl salt crystals crystallized at (D) 90°C, (E) 85°C, (F) 80°C, (G) 70°C, (H) 60°C, and (I) 50°C to show control over porogen size (salt concentration 0.38 g/mL).

SEM images of NaCl porogens nucleated at 90°C, 85°C, 80°C, 70°C, 60°C, and 50°C at a fixed concentration of 0.38 g/mL. The results show that as the nucleation temperature was reduced, the resulting NaCl crystal increased in size due to the reduction in free energy of the solution. The salt sizes produced ranged from 2.59 ± 0.90 μm at 90°C up to 95.39 ± 11.46 μm at 50°C (Fig. 3A). As the results show, the resulting NaCl porogen size can be precisely controlled within a narrow range to meet the needs for specific tissue engineering applications where the pore sizes must be consistent. Although the results show a maximum size of 106 μm, increased sizes can be obtained by lowering the nucleation temperature. Salt sizes as small as 461.56 ± 98.86 nm can be produced when nucleated at 99°C at 0.38 g/mL, showing the ability to produce porogens in the nanoscale range.

Adjusting the supersaturation concentration can also control the NaCl porogen size. Figure 3B shows the results from the NaCl porogen study in which the supersaturation concentration was increased from 0.30 up to 0.39 g/mL with a fixed nucleation temperature of 80°C. As the supersaturation concentration was increased from 0.30 to 0.39 g/mL, the resulting porogen size increased from 5.74 ± 0.57 to 68.23 ± 5.49 μm, respectively. In addition, the nucleation time was also controlled to evaluate the effects on NaCl crystal size. Figure 3C shows a correlation between the increased nucleation time and resulting crystal size. Thus, similar to using the temperature to control the porogen size, the concentration of the supersaturated solution and crystallization time can be used as an additional method to fine-tune the NaCl size within a narrow range.

When compared with traditional grinding and sieving methods to produce NaCl porogens, the nucleation and crystallization technique provides superior control over the resulting size distribution. Figure 4A shows the SEM images of NaCl produced after being sieved through a 50 μm sieve, and ground using a coffee grinder to produce even smaller porogen sizes. We believe that the method will produce the smallest porogen sizes possible in normal laboratory settings without the use of expensive equipment. Figure 4B shows the SEM images of NaCl nucleated at a concentration of 0.33 g/mL and 80°C. The results show that the grinding and sieving methods produce NaCl porogens 13.89 ± 12.49 μm, whereas the nucleation and crystallization method produced NaCl porogens 13.78 ± 1.18 μm

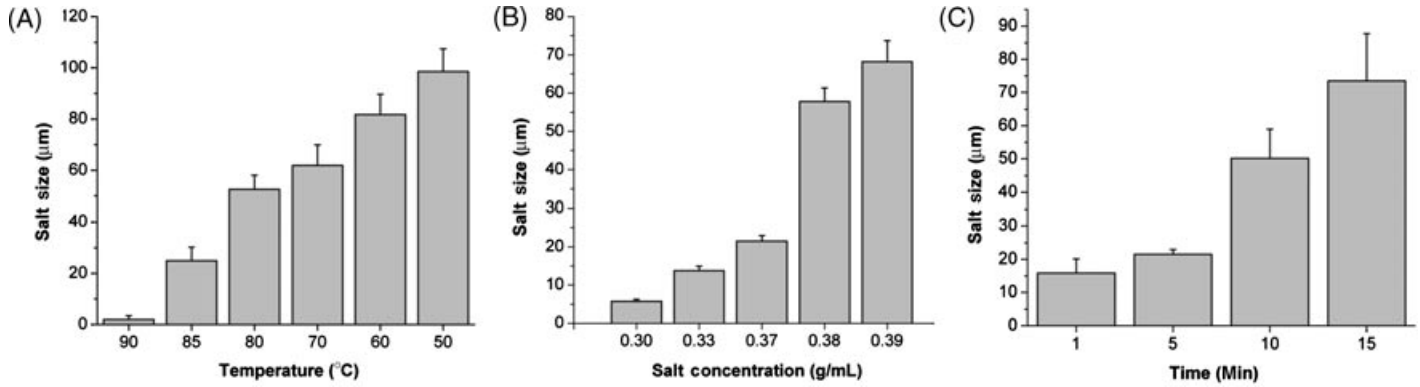

Fig. 3. Resulting NaCl crystal sizes obtained by crystallizing at various (A) nucleation temperatures (salt concentration 0.38 g/mL), (B) NaCl concentrations (nucleation temperature 80°C), and (C) nucleation times (salt concentration 0.37 g/mL and nucleation temperature 80°C).

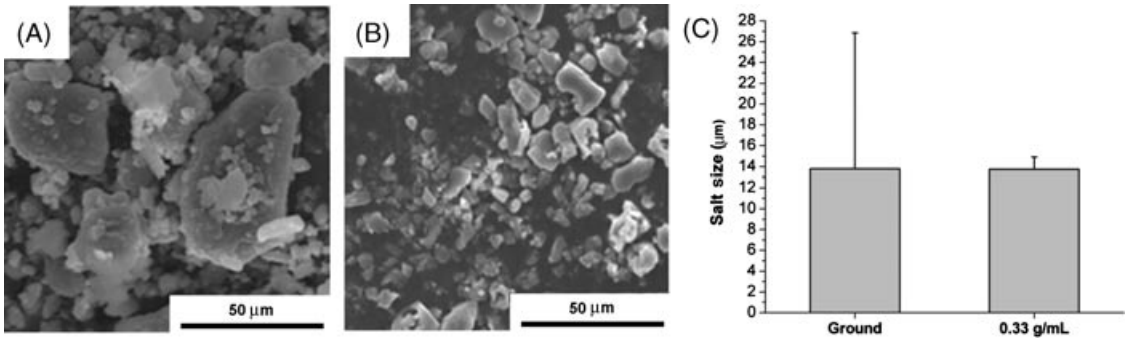

Fig. 4. SEM images of (A) traditional sieved and ground NaCl, (B) crystallized NaCl at a concentration of 0.33 g/mL at 80°C, and (C) graphical representation of the sieved and ground salt versus salt obtained from the nucleation and crystallization methods. No significant difference in NaCl crystal size was seen ($P > 0.05$); however, crystallization provides better control over the size variations.

(Fig. 4C). No significant difference in the mean size was seen between the two methods due to the large size distribution of the grinding method ($P > 0.05$). However, the nucleation and crystallization method allows for the generation of porogen sizes with a narrow size distribution, which will be beneficial in creating tissue engineering scaffolds with uniform pore sizes throughout the construct.

Tissue engineering scaffolds produced by traditional salt leaching methods typically are plagued by the presence of "dead" pores, which hinder cell–cell communication, mass transport, and cell infiltration. Figure 5A shows a SEM image of a CUPE 1.2 scaffold prepared using traditional salt leaching methods. Figure 5B shows the pore structure, which reveals the closed walls and dead pores. The interconnectivity index of the scaffold was measured as 2.98 $\pm$ 0.67%. When NaCl porogens produced from the nucleation and crystallization methods were incorporated with the traditional salt leaching methods, the interconnectivity was greatly improved. Figures 5C and 5D show the SEM images from CUPE 1.2 scaffolds created using both traditional and nucleation techniques to prepare scaffolds with improved interconnectivity with the potential for enhanced cell–cell communication and mass transport, which play a large role in the overall success of a tissue engineering scaffold. For example, studies have shown that the reciprocal interactions from the cell–cell communication between endothelial cells and mesenchymal stem cells have shown promise in generating vascularized bone–tissue engineering constructs [71]. Scaffolds created from this method showed an interconnectivity index of 19.17 $\pm$ 2.91%, which shows a great improvement over the previous traditional scaffold fabrication technique ($P < 0.01$). The pore morphology of the interconnected scaffolds also shows microscale and nanoscale topographies, which can be beneficial in reproducing surfaces that better mimic the native ECM for enhanced cell adhesion and differentiation. As the pore interconnectivity is an important aspect and plays a large role in the success of tissue engineering scaffolds, future research will focus on the use of alternative approaches such as mercury intrusion porosimetry [72], 3D microtomography [73], or 2D image analyses [74] to provide an improved quantification evaluation of the pore interconnection.

The nucleation and crystallization porogen method allowed for the fabrication of uniform porogen sizes smaller than traditional methods, which can be used in MEMS-based tissue-engineering applications. MEMS technologies have

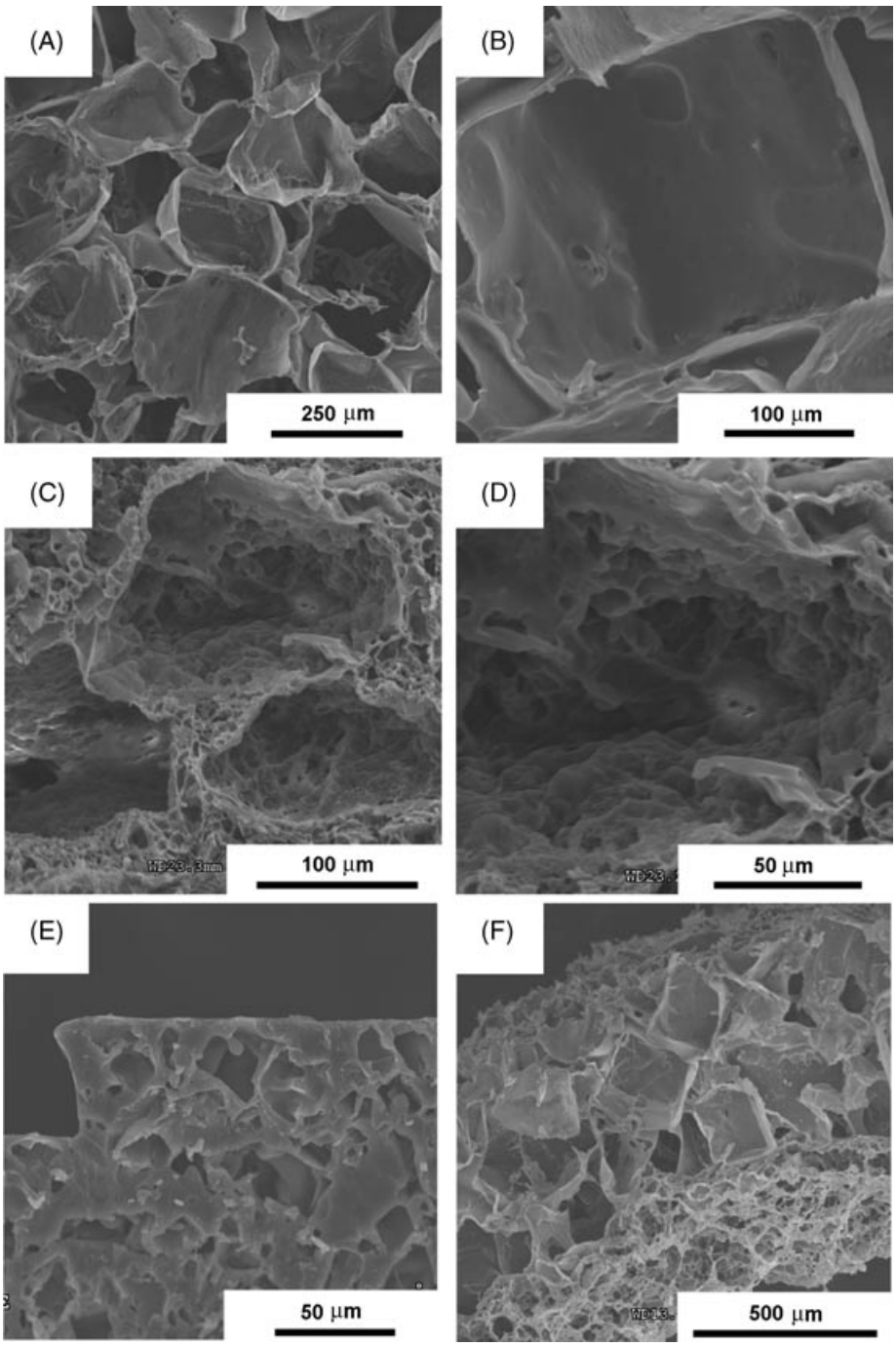

Fig. 5. SEM images of crosslinked urethane-doped polyester (CUPE) scaffolds prepared using only sieved 150–250 μm salt (A) 100 × and (B) 250 × to show the presence of dead pores. SEM images of CUPE scaffolds prepared using 150–250 μm salt in combination with crystallized submicron NaCl porogens to increase scaffold interconnectivity (C) 200 × and (D) 600 × . Cross-sectional SEM images of CUPE (E) porous microchanneled scaffolds and (F) multiphasic small diameter vascular grafts using submicron salt obtained from the nucleation and crystallization method.

recently been used with hydrogels and biodegradable elastomers to fabricate 3D structures with the ability to control cell adhesion, cell morphology, and create microvasculature using the physical cues of the construct to influence cell behavior [75–77]. Porous microchanneled MEMS scaffolds offer unique advantages in that cells can be evenly seeded onto the channels, the seeded scaffolds can be stacked together to form complex heterogeneous tissue constructs, the submicron porosity of the scaffold can allow for cell communication without cell migration into different layers, and the microchannel space can allow for nutrient supply through culture medium perfusion and influence cell organization by aligning the cells using contact guidance [78]. However, the introduction of submicron pores into MEMS-based scaffolds for cell communication while

preventing cell migration has been primarily accomplished using TIPS techniques [79]. Figure 5E shows the SEM image of porous microchanneled CUPE 1.2 scaffolds using MEMS-based techniques in combination with nucleation and crystallization pore generation methods. Through this new pore generation technique, submicron porosity can now be introduced into MEMS-based techniques. Although only CUPE was used as the material to fabricate porous scaffolds in this study, the nucleation and crystallization pore generation technique can potentially be applied to a wider selection of available materials to accommodate for the strict requirements of engineering various tissues.

We have also shown the fabrication of novel small diameter grafts using the nucleation and crystallization pore generation technology for vascular tissue engineering. To recreate the stratified cellular architecture of native vessels, we have proposed the fabrication of anatomically correct multiphasic small diameter grafts. As shown in Fig. 5F, we have constructed vascular grafts with two distinct layers: 1) a microporous luminal permeable elastic membrane to promote graft endothelialization while allowing for cell communication and 2) a porous tunica medial layer for smooth muscle and fibroblast cell proliferation. We believe that a small diameter vascular graft created with this type of distinct layered architecture will better mimic the native vessel anatomy to potentially improve graft function. In native blood vessels, endothelial cells and smooth muscle cells influence each other via the signaling molecules secreted by both cell types [80–84] through the internal elastic lamina. The failure of previously developed vascular grafts has been correlated with the lack of a functional endothelial luminal layer due to inappropriate luminal topographies, which result in graft thrombosis and neointimal hyperplasia [85]. The microporous luminal layer created using the nucleation and crystallization methods will provide the topography necessary for endothelial cell adhesion and proliferation while allowing for endothelial and smooth muscle cell communication. This scaffold fabrication method in combination with nucleation and crystallization pore generation technology provides a new avenue to fabricate complex heterogeneous porous scaffolds with different porosities, pore sizes, pore shapes, and interconnectivity among each layer to accommodate for specific cell types in the regeneration of multicellular tissues such as skin, blood vessels, liver, pancreas, and cartilage where the compartmentalization of different cell types is necessary [49],[86],[87].

4. Conclusion

A new generation of NaCl porogen has been developed for tissue engineering scaffold fabrication using the principles behind nucleation and crystallization science. This new porogen technology provides a facile, convenient, more precise, and cost-effective method over traditional sieving and grinding techniques to generate NaCl porogens within a narrow size range, which can be applied to a wide variety of biomaterials. The submicron NaCl porogens created using this new technique were used to fabricate porous and elastic multiphasic small diameter vascular grafts and microchanneled scaffolds for potential use in soft tissue engineering applications. This new pore generation technique may serve as a powerful tool and add to the current repertoire of tissue engineering scaffold design methods.

Acknowledgements

This work was supported in part by a beginning grant-in-aid award from the American Heart Association, award R21EB009795 from the National Institute of Biomedical Imaging and Bioengineering, high impact/high risk award RP110412 from Cancer Prevention and Research Institute of Texas, and the National Science Foundation CAREER award 0954109.

References

[1] Langer, R., and Vacanti, J. P. (1993) *Science* **260**, 920–926.
[2] Cima, L. G., Vacanti, J. P., Vacanti, C., Ingber, D., Mooney, D., and Langer, R. (1991) *J. Biomech. Eng.* **113**, 143–151.
[3] Mansbridge, J. N. (2009) *Curr. Opin. Biotechnol.* **20**, 563–567.
[4] Cancedda, R., Giannoni, P., and Mastrogiacomo, M. (2007) *Biomaterials* **28**, 4240–4250.
[5] Marcacci, M., Berruto, M., Brocchetta, D., Delcogliano, A., Ghinelli, D., Gobbi, A., Kon, E., Pederzini, L., Rosa, D., Sacchetti, G. L., Stefani, G., and Zanasi, S. (2005) *Clin. Orthop. Relat. Res.* 96–105.
[6] Calve, S., Dennis, R. G., Kosnik, P. E., 2nd, Baar, K., Grosh, K., and Arruda, E. M. (2004) *Tissue Eng.* **10**, 755–761.
[7] Vunjak-Novakovic, G., Altman, G., Horan, R., and Kaplan, D. L. (2004) *Annu. Rev. Biomed. Eng.* **6**, 131–156.
[8] Kulig, K. M., and Vacanti, J. P. (2004) *Transpl. Immunol.* **12**, 303–310.
[9] Jawad, H., Ali, N. N., Lyon, A. R., Chen, Q. Z., Harding, S. E., and Boccaccini, A. R. (2007) *J. Tissue Eng. Regen. Med.* **1**, 327–342.
[10] Koike, N., Fukumura, D., Gralla, O., Au, P., Schechner, J. S., and Jain, R. K. (2004) *Nature* **428**, 138–139.
[11] Penkala, R. A., and Kim, S. S. (2007) *Expert Rev. Med. Devices* **4**, 65–72.
[12] Stosich, M. S., and Mao, J. J. (2007) *Plast. Reconstr. Surg.* **119**, 71–83.
[13] Fiegel, H. C., Kaufmann, P. M., Bruns, H., Kluth, D., Horch, R. E., Vacanti, J. P., and Kneser, U. (2008) *J. Cell Mol. Med.* **12**, 56–66.
[14] Wagner, W. R. and Griffith, B. P. *Science* **329**, 520–522.
[15] Chalfoun, C. T., Wirth, G. A., and Evans, G. R. (2006) *J. Cell Mol. Med.* **10**, 309–317.
[16] Sachlos, E., and Czernuszka, J. T. (2003) *Eur. Cell Mater.* **5**, 29–39; discussion 39–40.
[17] Ayres, C. E., Jha, B. S., Sell, S. A., Bowlin, G. L., and Simpson, D. G. *Wiley Interdiscip. Rev. Nanomed. Nanobiotechnol.* **2**, 20–34.
[18] Hollister, S. J. (2005) *Nat. Mater.* **4**, 518–524.
[19] Li, W. J., Laurencin, C. T., Caterson, E. J., Tuan, R. S., and Ko, F. K. (2002) *J. Biomed. Mater. Res.* **60**, 613–621.
[20] Tran, R., Thevenot, P., Gyawali, D., Chiao, J., Tang, L., and Yang, J. (2010) *Soft Matter.* **6**, 2449–2461.
[21] Smith, I. O., Liu, X. H., Smith, L. A., and Ma, P. X. (2009) *Wiley Interdiscip. Rev. Nanomed. Nanobiotechnol.* **1**, 226–236.
[22] O'Brien, F. J., Harley, B. A., Yannas, I. V., and Gibson, L. J. (2005) *Biomaterials* **26**, 433–441.
[23] Hutmacher, D. W., Schantz, T., Zein, I., Ng, K. W., Teoh, S. H., and Tan, K. C. (2001) *J. Biomed. Mater. Res.* **55**, 203–216.
[24] Zeltinger, J., Sherwood, J. K., Graham, D. A., Mueller, R., and Griffith, L. G. (2001) *Tissue Eng.* **7**, 557–572.
[25] O'Brien, F. J., Harley, B. A., Yannas, I. V., and Gibson, L. (2004) *Biomaterials* **25**, 1077–1086.
[26] Galperin, A., Long, T. J., and Ratner, B. D. (2010) *Biomacromolecules* **11**, 2583–2592.
[27] Murphy, W. L., Dennis, R. G., Kileny, J. L., and Mooney, D. J. (2002) *Tissue Eng.* **8**, 43–52.
[28] Lee, J., Lee, H., Kim, J., Hyon, S., and Kim, S. (2003) *J. Appl. Polym. Sci.* **88**, 2224–2232.

[29] Young, T. H., Lin, C. W., Cheng, L. P., and Hsieh, C. C. (2001) *Biomaterials* **22**, 1771–1777.
[30] Krasteva, N., Seifert, B., Albrecht, W., Weigel, T., Schossig, M., Altankov, G., and Groth, T. (2004) *Biomaterials* **25**, 2467–2476.
[31] Coombes, A. G., Rizzi, S. C., Williamson, M., Barralet, J. E., Downes, S., and Wallace, W. A. (2004) *Biomaterials* **25**, 315–325.
[32] Sarazin, P., Roy, X., and Favis, B. D. (2004) *Biomaterials* **25**, 5965–5978.
[33] Roychowdhury, P., and Kumar, V. (2006) *J. Biomed. Mater. Res. A.* **76**, 300–309.
[34] Salerno, A., Oliviero, M., Di Maio, E., Iannace, S., and Netti, P. A. (2009) *J. Mater. Sci. Mater. Med.* **20**, 2043–2051.
[35] Haugen, H., Ried, V., Brunner, M., Will, J., and Wintermantel, E. (2004) *J. Mater. Sci. Mater. Med.* **15**, 343–346.
[36] Zhu, X. H., Lee, L. Y., Jackson, J. S., Tong, Y. W., and Wang, C. H. (2008) *Biotechnol. Bioeng.* **100**, 998–1009.
[37] Maio, E., Mensitieri, G., Iannace, S., Nicolais, L., Li, W., and Rlumerfeit, R. (2005) *Polym. Eng. Sci.* **45**, 432–441.
[38] Jessop, P. G., and Subramaniam, B. (2007) *Chem. Rev.* **107**, 2666–2694.
[39] Xu, Q., Ren, X., Chang, Y., Wang, J., Yu, L., and Dean, K. (2004) *J. Appl. Polym. Sci.* **94**, 593–597.
[40] Barry, J. J., Gidda, H. S., Scotchford, C. A., and Howdle, S. M. (2004) *Biomaterials* **25**, 3559–3568.
[41] Nam, Y. S., Yoon, J. J., and Park, T. G. (2000) *J. Biomed. Mater. Res.* **53**, 1–7.
[42] Sun, W., Darling, A., Starly, B., and Nam, J. (2004) *Biotechnol. Appl. Biochem.* **39**, 29–47.
[43] Peltola, S. M., Melchels, F. P., Grijpma, D. W., and Kellomaki, M. (2008) *Ann. Med.* **40**, 268–280.
[44] Liu, C. Z., Xia, Z. D., Han, Z. W., Hulley, P. A., Triffitt, J. T., and Czernuszka, J. T. (2008) *J. Biomed. Mater. Res. B. Appl. Biomater.* **85**, 519–528.
[45] Xu, M., Li, Y., Suo, H., Yan, Y., Liu, L., Wang, Q., Ge, Y., and Xu, Y. *Biofabrication* **2**, 025002.
[46] Cao, T., Ho, K. H., and Teoh, S. H. (2003) *Tissue Eng.* **9**(Suppl 1), S103–S112.
[47] Yeong, W. Y., Sudarmadji, N., Yu, H. Y., Chua, C. K., Leong, K. F., Venkatraman, S. S., Boey, Y. C., and Tan, L. P. *Acta Biomater.* **6**, 2028–2034.
[48] Yeong, W. Y., Chua, C. K., Leong, K. F., and Chandrasekaran, M. (2004) *Trends Biotechnol.* **22**, 643–652.
[49] Hutmacher, D. W. (2000) *Biomaterials* **21**, 2529–2543.
[50] Cheah, C. M., Chua, C. K., Leong, K. F., Cheong, C. H., and Naing, M. W. (2004) *Tissue Eng.* **10**, 595–610.
[51] Weigel, T., Schinkel, G., and Lendlein, A. (2006) *Expert Rev. Med. Devices* **3**, 835–851.
[52] Ma, Z., Kotaki, M., Inai, R., and Ramakrishna, S. (2005) *Tissue Eng.* **11**, 101–109.
[53] Yang, J., Webb, A. R., Pickerill, S. J., Hageman, G., and Ameer, G. A. (2006) *Biomaterials* **27**, 1889–1898.
[54] Tran, R., Thevenot, P., Zhang, Y., Tang, L., and Yang, J. (2010) *Soft Matter.* **6**, 2449–2461.
[55] Gyawali, D., Nair, P., Zhang, Y., Tran, R. T., Zhang, C., Samchukov, M., Makarov, M., Kim, H. K., and Yang, J. *Biomaterials* **31**, 9092–9105.
[56] Gyawali, D., Tran, R. T., Guleserian, K. J., Tang, L., and Yang, J. *J. Biomater. Sci. Polym. Ed.* **21**, 1761–1782.
[57] Wang, Y., Kim, Y. M., and Langer, R. (2003) *J. Biomed. Mater. Res. A.* **66**, 192–197.
[58] Nam, Y. S., and Park, T. G. (1999) *J. Biomed. Mater. Res.* **47**, 8–17.
[59] Liao, C. J., Chen, C. F., Chen, J. H., Chiang, S. F., Lin, Y. J., and Chang, K. Y. (2002) *J. Biomed. Mater. Res.* **59**, 676–681.
[60] Ma, Z., Gao, C., Gong, Y., and Shen, J. (2003) *J. Biomed. Mater. Res. B. Appl. Biomater.* **67**, 610–617.
[61] Capes, J. S., Ando, H. Y., and Cameron, R. E. (2005) *J. Mater. Sci. Mater. Med.* **16**, 1069–1075.
[62] Draghi, L., Resta, S., Pirozzolo, M. G., and Tanzi, M. C. (2005) *J. Mater. Sci. Mater. Med.* **16**, 1093–1097.
[63] Hoshi, R., Behl, S., and Ameer, G. (2009) *Advanced Mater.* **21**, 188–192.
[64] Leubner, I. (2010) *Precision Crystallization*. CRC Press, Boca Raton, FL.
[65] Pechkova, E., Gebhardt, R., Riekel, C., and Nicolini, C. *Biophys. J.* **99**, 1256–1261.
[66] Galindo, H. M., Carvajal, Y., Njagi, E., Ristau, R. A., and Suib, S. L. *Langmuir* **26**, 13677–13683.
[67] De Yoreo, J. J., and Vekilov, P. G. (2003) *Reviews in Mineralogy and Geochemistry* **54**, 57–93.
[68] Dey, J., Xu, H., Shen, J., Thevenot, P., Gondi, S. R., Nguyen, K. T., Sumerlin, B. S., Tang, L., and Yang, J. (2008) *Biomaterials* **29**, 4637–4649.
[69] Yang, J., Shi, G., Bei, J., Wang, S., Cao, Y., Shang, Q., Yang, G., and Wang, W. (2002) *J. Biomed. Mater. Res.* **62**, 438–446.
[70] Mathew, J. A., Kache, V., Liu, C., Tang, L., and Yang, J. (2007) *IEEE Dallas* 11–12, 43–46.
[71] Grellier, M., Bordenave, L., and Amedee, J. (2009) *Trends Biotechnol.* **27**, 562–571.
[72] Tully-Dartez, S., Cardenas, H. E., and Sit, P. F. *Tissue Eng. Part C Methods* **16**, 339–345.
[73] Jones, A. C., Arns, C. H., Hutmacher, D. W., Milthorpe, B. K., Sheppard, A. P., and Knackstedt, M. A. (2009) *Biomaterials* **30**, 1440–1451.
[74] Guarino, V., Guaccio, A., Netti, P. A., and Ambrosio, L. *J. Mater. Sci. Mater. Med.* **21**, 3109–3118.
[75] Bashir, R. (2004) *Adv. Drug Deliv. Rev.* **56**, 1565–1586.
[76] Puleo, C. M., Yeh, H. C., and Wang, T. H. (2007) *Tissue Eng.* **13**, 2839–2854.
[77] Peppas, N. A., Hilt, J. Z., Khademhosseini, A., and Langer, R. (2006) *Advanced Materials* **18**, 1345–1360.
[78] Papenburg, B. J., Liu, J., Higuera, G. A., Barradas, A. M., de Boer, J., van Blitterswijk, C. A., Wessling, M., and Stamatialis, D. (2009) *Biomaterials* **30**, 6228–6239.
[79] Papenburg, B. J., Vogelaar, L., Bolhuis-Versteeg, L. A., Lammertink, R. G., Stamatialis, D., and Wessling, M. (2007) *Biomaterials* **28**, 1998–2009.
[80] Fillinger, M. F., Sampson, L. N., Cronenwett, J. L., Powell, R. J., and Wagner, R. J. (1997) *J. Surg. Res.* **67**, 169–178.
[81] Davies, P. F. (1986) *Lab. Invest.* **55**, 5–24.
[82] Lyubimov, E. V., and Gotlieb, A. I. (2004) *Cardiovasc. Pathol.* **13**, 139–145.
[83] Williams, C., and Wick, T. M. (2005) *Annals. Biomed. Eng.* **33**, 920–928.
[84] Hisano, N., Yatomi, Y., Satoh, K., Akimoto, S., Mitsumata, M., Fujino, M. A., and Ozaki, Y. (1999) *Blood* **93**, 4293–4299.
[85] Brown, M. A., Zhang, L., Levering, V. W., Wu, J. H., Satterwhite, L. L., Brian, L., Freedman, N. J., and Truskey, G. A. (2010) *Arterioscler. Thromb. Vasc. Biol.* **30**, 2150–2155.
[86] Yang, J., Motlagh, D., Webb, A. R., and Ameer, G. A. (2005) *Tissue Eng.* **11**, 1876–1886.
[87] Ryu, W., Min, S. W., Hammerick, K. E., Vyakarnam, M., Greco, R. S., Prinz, F. B., and Fasching, R. J. (2007) *Biomaterials* **28**, 1174–1184.